Title: High-throughput CRISPR screens to dissect macrophage-*Shigella* interactions

Authors: Yong Lai[1,2,3], Liang Cui[1], John G. Doench[4], & Timothy K. Lu[1-7*]

Affiliations: [1]Antimicrobial Resistance Interdisciplinary Research Group, Singapore-MIT Alliance for Research and Technology, Singapore; [2]Synthetic Biology Group, MIT Synthetic Biology Center, Massachusetts Institute of Technology (MIT), Cambridge, MA, USA; [3]Research Laboratory of Electronics, MIT, Cambridge, MA, USA; [4]Broad Institute, Cambridge, MA, USA; [5]Department of Electrical Engineering and Computer Science, MIT, Cambridge, MA, USA; [6]Harvard-MIT Division of Health Sciences and Technology, Cambridge, MA, USA; [7]Department of Biological Engineering, MIT, Cambridge, MA, USA.

*e-mail: timlu@mit.edu

Shigellosis, the primary cause of diarrheal deaths worldwide, particularly affects children living in low and middle-income countries[1]. The causative agent, *Shigella* spp., invades and replicates in the epithelium of the large intestine, eliciting an intense inflammatory response and tissue destruction[2]. However, how *Shigella* rewires macrophages prior to epithelial cell invasion[3] is poorly understood. Here we show that *Shigella flexneri* induces the production of pro-inflammatory cytokines and chemokines and triggers host pyruvate catabolism for energy acquisition before rapidly killing macrophages. To identify host factors modulated by *S. flexneri*, we performed genome-wide and focused secondary CRISPR knockout and CRISPRi

screens in human monocytic THP-1 cells infected with *S. flexneri* and evaluated host cell survival. Knockdown of key components of the Toll-like receptor 1/2 signaling pathway significantly reduced pro-inflammatory cytokine and chemokine production, enhanced host cell survival, and controlled intracellular pathogen growth. Knockdown of the enzymatic component of the mitochondrial pyruvate dehydrogenase complex also enhanced THP-1 cell survival. Small molecule inhibitors, which selectively inhibit key components of these pathways, enhanced host survival and limited intracellular pathogen growth. High-throughput CRISPR screens provide insights into the specific effects of *S. flexneri* on macrophages; these insights can potentially guide development of new therapies for shigellosis.

Annually, there are more than one million cases of shigellosis[1]. In 2016, over two hundred thousand people were killed by shigellosis globally[4]. More than 65% of these deaths occurred in children under 5 years old and in adults older than 70 years[4], indicating that the fully developed, healthy human immune system may be sufficient to prevent and control *Shigella* infections. We therefore investigated susceptibility to this potentially lethal bacterium at the cellular level, focusing on immune cells.

Infection is initiated when *Shigella* crosses the intestinal epithelium through microfold cells (M cells)[5]. After transcytosis to the M cell pocket, *Shigella* targets the resident macrophages, inducing caspase-1-dependent pyroptotic cell death, an essential step to subsequent invasion and replication in the intestinal epithelium[3,6]. Epithelial cells constitute the major habitat of *Shigella*[7]. Within this replicative niche, *Shigella flexneri* delivers various virulence proteins via a type III secretion system (T3SS), resulting in weakened host defenses[7]. These virulence proteins reduce intracellular trafficking[8,9],

antagonize caspase-4-dependent pyroptosis[10], prevent necrosis mediated by mitochondrial damage[11], and inhibit the early stage of apoptosis by p53 degradation[12]. As a consequence, epithelial cells survive infection and continue to harbor the bacteria[12-14].

Whereas the effects of *Shigella* infection on epithelial cells have been studied extensively, little attention has been paid to how *S. flexneri* interacts with macrophages, although it has been demonstrated that this intracellular pathogen rapidly induces macrophage pyroptosis by activating NLRP3- or NLRC4-inflammasomes[15-17]. To improve our understanding of how *S. flexneri* manipulates macrophages and induces rapid cell death and to identify host targets for potential therapy, we conducted CRISPR screens in human macrophage-like THP-1 cells following infection with *S. flexneri*.

To examine whether *S. flexneri* infects and kills THP-1 cells, we first assessed the phagocytosis of *S. flexneri* M90T by detecting the red fluorescence (*uhpT*::dsRed) induced by host cell-produced glucose 6-phosphate[18] and indicative of intracellular *S. flexneri*. We then measured THP-1 cell viability post-infection (Extended Data Fig. 1). We found that *S. flexneri*, at a multiplicity of infection (MOI) of 10:1, efficiently infected THP-1 cells and induced host cell death 3 hours after infection (Extended Data Fig. 1a, d, e). Such infection with *S. flexneri* can be utilized as selective pressure for subsequent host survival-based genetic screens. Independent biological triplicates of genome-wide CRISPR knockout and CRISPRi screen libraries were prepared in THP-1 cells expressing Cas9 and dCas9-Krab, respectively[19-21] (Extended Data Fig. 2). After *S. flexneri* infection, surviving THP-1 cells with specific sgRNA barcodes were maintained in culture medium for continuous replication and harvested for next generation sequencing and analysis. The distribution of sgRNAs in *S. flexneri*-infected THP-1 cells was significantly different from that in

uninfected THP-1 cells (Extended Data Fig. 3). The results of genome-wide screens were visualized with volcano plots (Fig. 1a, b).

In order to identify top positively selected genetic hits in *S. flexneri*-infected THP-1 cells, we used a false discovery rate (FDR) of <0.25 and log2 fold change of >1 as cut-off points. Positive hits were considered those that extended the survival of the THP-1 cells after 2-3 hours of bacterial infection. We observed positive selection of 76 and 28 genes in CRISPR-Cas9 knockout and CRISPRi screens, respectively, with 10 genes enriched in both screens (p-value <7.394E-18; Fig. 1c; Supplementary Tables 1 and 2). Pathway analysis identified multiple enriched biological processes in *S. flexneri*-infected THP-1 cells. Both CRISPR-Cas9 knockout and CRISPRi screens identified the same pathways, such as Toll-like receptor (TLR) cascades, chromatin organization, pyruvate catabolism, the cellular stress response pathway, and receptor tyrosine kinase signaling (Fig. 1d, e; Extended Data Fig. 4a, b). More specifically, all key components of the TLR1/2 signaling pathway (TRAF6, IRAK1, IRAK4, MYD88, TLR1, TLR2, TIFA, TIRAP) were identified in our genome-wide screens (Fig. 1f). Intriguingly, TRAF6 and TIFA also play important roles in the ALPK1-TIFA-TRAF6-NF-κB pathway, by which epithelial cells detect lipopolysaccharide (LPS) biosynthetic intermediates and regulate inflammation in response to them[22-24]. Yet, ALPK1, a newly identified cytosolic immune receptor in *Yersinia pseudotuberculosis* and *S. flexneri* infection[23,25], was not a genetic hit in our genome-wide CRISPR screens (Fig. 1f). Although *S. flexneri* causes NF-κB-induced inflammation in both macrophages and epithelial cells, it also exhibits distinct mechanisms of host manipulation that may contribute to opposite outcomes of infection in these cell

types, i.e., rapidly induced cell death of macrophages but inhibited cell death of epithelial cells[7].

Moreover, the identification of genes involved in pyruvate catabolism (PDHB, DLAT, CS, PDHA1, MPC1, MPC2; Fig. 1f) echoed the rerouting of carbon flux by *S. flexneri* observed in HeLa cells[26], which supports the rapid growth of these bacteria in this host. Intriguingly, key components of the NLRC4 and NLRP3 inflammasomes (AIM2, CASP1, NLRC4, NLRP3, GSDMD, and NAIP) that are activated by *S. flexneri* T3SS effectors MxiI[17], IpaB[27], and IpaH7.8[28] in macrophages were identified as negative hits in our genome-wide CRISPR screens (i.e., a gene whose knockout or knockdown shortened THP-1 cell survival) (Fig. 1f), indicating that certain genes in the pyroptotic cell death pathway may actually protect host cells in *S. flexneri* infection. Overall, our results indicate the reliability of genome-wide CRISPR screens for studying *S. flexneri* infection and the importance of comprehensively understanding macrophage-*S. flexneri* interactions.

We next designed and prepared secondary CRISPR knockout and CRISPRi screen libraries targeting 372 human genes in order to validate genome-wide screen hits[21], to test genes that were associated with different types of host cell death, and to compare the performance between CRISPR knockout and knockdown libraries by ensuring that there were consistent numbers of sgRNAs per gene in each type of library. Similar to our genome-wide screens, surviving THP-1 cells were harvested following *S. flexneri* infection, and the results of the screens were visualized with volcano plots (Extended Data Fig. 5a, b). We identified 23 and 29 genes in secondary CRISPR knockout and CRISPRi screens, respectively, with 12 genes enriched in both screens (FDR<0.05; log2 FC>0.5; p-value<3.486E-09; Fig. 2a). To evaluate the reliability of our genome-wide CRISPR screens,

we calculated the validation rate of genes in secondary screens based on the FDR threshold (<5%); these genes were clustered by their p-value in the genome-wide screens[20] (Fig. 2b). The validation rate of screen hits in secondary CRISPR knockout and CRISPRi screens decreased with increasing p-values in primary genome-wide screens. This result suggests the reliability of genome-wide screens, which have lower numbers of sgRNAs per gene than secondary screen libraries, for studying bacterial infections (Extended Data Fig. 2). Furthermore, genome-wide top positive genetic hits were validated by secondary screens, such as genes in the TLR1/2 signaling pathway (IRAK1, MYD88, TRAF6), the type I interferon pathway (TYK2, IFNAR2, IRF8, STAT2), and the TNF receptor signaling pathway (TNFRSF1A), suggesting the robustness of genome-wide screens (Fig. 2c; Extended Data Fig. 5c; Supplementary Tables 3 and 4). Yet, genes involved in pyruvate catabolism, such as PDHB and PDHA1, were not scored significantly in secondary screens (Extended Data Fig. 5c); further validation of these genes would be required to confirm their involvement in the infectious process. Positive screen hits that were identified by both genome-wide and secondary screens were summarized based on the diverse signaling pathways they are associated with in *S. flexneri* infection (Fig. 2d). Many positive genetic hits with unknown functions in bacterial infection were also identified (PHF6, PHIP, TRERF1, and MAP2K7).

Consistent with genome-wide CRISPR screens, components of inflammasomes mediating pyroptosis in macrophages post-infection, such as NLRP3 and GSDMD, were identified in our secondary screens as negative hits (Fig. 2d; Extended Data Fig. 5c). Yet, genes involved in other types of host cell death, i.e., necrosis and apoptosis, did not show consistent patterns of screen phenotypes and were not identified as genetic hits. Not

surprisingly, NOD1, a critical intracellular bacterial sensor, was identified as a negative hit in the CRISPR knockout screen, indicating its protective role for host cells (Fig. 2d; Extended Data Fig. 5c). Intriguingly, SOD1 and SOD2, which destroy free superoxide radicals in host cells, were also identified as negative screen hits in *S. flexneri* infections (Fig. 2d; Extended Data Fig. 5c); decreased expression of these genes may contribute to necrosis induced by reactive oxygen species[29]. Additionally, by calculating the sgRNA correlation of replicates, signal/noise ratio, p-value, and FDR of CRISPR screens, we found that CRISPR-Cas9 knockout and CRISPRi yielded comparable results in secondary screens (Extended Data Fig. 6).

To further verify the function of top positive genetic hits, we next constructed THP-1 cells with individual gene knockdowns and confirmed their phenotypes in *S. flexneri* infection. The positive correlation between screen phenotype and validation phenotype confirmed that repression of positive screen hits indeed enhanced host cell survival with a 92.3% true positive rate (Pearson R=0.56; Fig. 3a). Moreover, repression of the transcription of MYD88, TRAF6, and IRAK1, key components in the TLR1/2 signaling pathway, also inhibited intracellular *S. flexneri* growth (Fig. 3b).

To characterize how the inhibition of those positive genetic hits mediates the host cell response and provides protection, we measured cytokine and chemokine production regulated by the TLR1/2 signaling pathway (Fig. 3c). Knockdown of the transcription of either MYD88 or IRAK1 abolished the production of infection-induced pro-inflammatory cytokines and chemokines, such as IL-1β, IL-2, and IL-8 (Fig. 3d; Extended Data Fig. 7a). As a potential strategy to control intracellular bacterial infection by targeting host factors, we tested the function of corresponding small molecule inhibitors. IRAK1/4-Inh, a

selective inhibitor of IRAK1, inhibited *S. flexneri* growth and pro-inflammatory cytokine and chemokine production, and protected host cells in a dose-dependent manner (Fig. 3e, f; Extended Data Fig. 7b-d). Ginsenoside Compound K (CK), a metabolite of Panax ginseng that also inhibits IRAK1[30], similarly enhanced host cell survival, inhibited *S. flexneri* growth, and abolished infection-induced IL-8 production in THP-1 cells (Extended Data Fig. 8).

In addition to dysregulating the host immune response, *S. flexneri* grows rapidly and replicates in host cells but does so only if there is an adequate supply of nutrients. Knockout or knockdown of components of the pyruvate dehydrogenase complex or the pyruvate transporter MPC1/2 in the mitochondria redirected central metabolism, favoring the survival of THP-1 cells infected with *S. flexneri* (Fig. 2d, 4a), which is congruent with the induction by *S. flexneri* in HeLa cells of the production of acetyl-CoA[26]. We next tested the function of the PDHB inhibitor oxythiamine (OT), as well as its combination with an IRAK1 inhibitor (IRAK1/4-Inh), in *S. flexneri* infection. OT treatment enhanced host cell survival post-infection (Fig. 4b) but failed to control intracellular *S. flexneri* growth (Fig. 4c), which is consistent with the PDHB gene knockdown phenotype (Fig. 3a, b). Interestingly, the combination of both IRAK1 and PDHB inhibitors (IRAK1/4-Inh and OT) significantly enhanced host cell survival and controlled *S. flexneri* growth better than treatment with either of these inhibitors alone, indicating a synergistic effect of inhibitors targeting both immune and non-immune pathways in macrophages (Fig. 4b, c). Furthermore, in a PMA-stimulated THP-1- *S. flexneri* infection model, IRAK1/4-Inh, OT, and their combination enhanced host cell survival and limited intracellular pathogen growth (Fig. 4d-f).

In line with a previous study of HeLa cells[26], we found that *S. flexneri* induced acetyl-CoA production in THP-1 cells, suggesting that, in both cases, *S. flexneri* supports its own rapid intracellular growth and replication by manipulating the central metabolism of the host cell (Fig. 4g). Moreover, 0.1 mM of PDHB inhibitor decreased infection-induced acetyl-CoA and downstream succinate production, which shifts host metabolism and leads to enhanced host cell survival (Fig. 4g, h). The combination of both IRAK1 and PDHB inhibitors reduced acetyl-CoA and succinate production to the uninfected levels, thus limiting intracellular *S. flexneri* growth and propagation (Fig. 4g, h).

Rapid macrophage death is prerequisite for *S. flexneri* to further infect and persist in the surrounding epithelial cells, which ultimately results in diarrhea and even dysentery, the most life-threatening manifestations of infection. However, unlike the intensive studies of the effects of *Shigella* infection on epithelial cells, the comprehensive interactions between *S. flexneri* and macrophages have been largely overlooked[15-17,27,28]. Our study highlights the capability of host cell survival-based CRISPR screens to elucidate complex macrophage-pathogen interactions and to identify key cellular processes that are disrupted by intracellular pathogens. In epithelial cells, NF-κB-related inflammatory signaling is one of the major defenses against *S. flexneri* infection[23,24]. For instance, upon sensing ADP-β-D-manno-heptose (ADP-Hep), epithelial cells activate NF-κB signaling in their cytosol and produce the pro-inflammatory chemokine IL-8. In response to these signals, *S. flexneri* produces multiple virulence proteins, disrupting inflammation and preventing epithelial cell death.

However, what occurs in epithelial cells does not necessarily occur in other cell types. In fact, our study revealed effects of *S. flexneri* in macrophage-like THP-1 cells

206 distinct from those reported for *Shigella*-infected epithelial cells. In THP-1 cells, *S. flexneri*
207 also stimulated IL-8 production but did so by activating the TLR1/2 signaling pathway,
208 and infection induced rapid THP-1 cell death. Although the TLR1/2 pathway is well known
209 for its role in the innate immune response to invading pathogens via the recognition of
210 peptidoglycan and triacyl lipopeptides, the induced inflammation could contribute to
211 bacterial pathogenesis[31]. For instance, in *Burkholderia* infection, knockout of TLR2
212 enhances the survival of mice and reduces sepsis, compared to what was observed with
213 wild-type mice[32]. Moreover, blockade of both TLR2 and TLR4 with monoclonal antibodies
214 effectively inhibits *Escherichia coli* and *Salmonella enterica*-triggered immunopathology
215 and prevents mouse death[33]. In our study, inhibiting the TLR1/2 signaling pathway in THP-
216 1 cells by IRAK1 inhibitors reduced pro-inflammatory cytokine and chemokine production,
217 enhanced THP-1 cell survival, and limited intracellular *S. flexneri* growth and replication,
218 indicating the detrimental effect of the TLR1/2 signaling pathway in immune cells during
219 *S. flexneri* infection. Considering the opposite effects of NF-κB signaling when epithelial
220 cells and immune cells are infected with *S. flexneri*, modulating the inflammatory response
221 of the host as a therapeutic strategy should be very carefully considered.

222 It is well known that macrophage pyroptosis is triggered by *S. flexneri*, allowing
223 bacteria to escape from macrophages and invade epithelial cells[7]. But this process also
224 restricts intracellular bacterial pathogens by cytokine-independent mechanisms in a mouse
225 model[34] or by the direct antibacterial effect of GSDMD-NT (the N-terminal cleavage
226 product of GSDMD in pyroptosis)[35]. It has been unclear whether pyroptosis protects the
227 macrophages or the intracellular bacteria. Our host genetic perturbation strategies provide
228 direct causal evidence that some of the genes that contribute to pyroptosis actually benefit

the host cells, since knockout or knockdown of key components of pyroptosis (GSDMD and NLRP3) decreased host cell survival post-infection (Fig. 2d; Extended Data Fig. 5c).

Treatment for shigellosis is becoming increasingly difficult as resistance to most inexpensive and widely used antibiotics becomes more prevalent[36]. In order to reduce mortality from diarrhea in children under 5 years of age to less than 1/1000 live births by 2025[37], current antibiotics will have to be complemented by other kinds of treatment, such as host-directed therapies. Given that macrophages and epithelial cells appear to be manipulated by *S. flexneri* in diametrically opposite ways, developing an adjuvant therapy by targeting a common feature of those two types of host cells may be one way to block bacterial pathogenesis. In this study, we demonstrated that by inhibiting infection-induced acetyl-CoA production in host immune cells, the function of these cells can be restored and energy acquisition by the intracellular pathogen can be limited (Fig. 4). In summary, our study not only sheds new light on the mechanisms underlying macrophage-*S. flexneri* interactions but also provides new insights to guide the development of adjuvant therapy for shigellosis treatment.

References

1 Kotloff, K. L., Riddle, M. S., Platts-Mills, J. A., Pavlinac, P. & Zaidi, A. K. M. Shigellosis. *Lancet* **391**, 801-812 (2018).

2 Schroeder, G. N. & Hilbi, H. Molecular pathogenesis of *Shigella* spp.: controlling host cell signaling, invasion, and death by type III secretion. *Clin Microbiol Rev* **21**, 134-156 (2008).

3 Ashida, H. *et al. Shigella* deploy multiple countermeasures against host innate immune responses. *Curr Opin Microbiol* **14**, 16-23 (2011).

4 Khalil, I. A., Troeger, T. & Blacker, B. F. Morbidity and mortality due to *Shigella* and enterotoxigenic *Escherichia coli* diarrhoea: the Global Burden of Disease Study 1990-2016. *Lancet Infect Dis* **18**, 1305-1305 (2018).

5 Wassef, J. S., Keren, D. F. & Mailloux, J. L. Role of M-cells in initial antigen uptake and in ulcer formation in the rabbit intestinal loop model of shigellosis. *Infect Immun* **57**, 858-863 (1989).

6 Ashida, H., Kim, M. & Sasakawa, C. Manipulation of the host cell death pathway by *Shigella*. *Cell Microbiol* **16**, 1757-1766 (2014).

7 Ashida, H., Mimuro, H. & Sasakawa, C. *Shigella* manipulates host immune responses by delivering effector proteins with specific roles. *Front Immunol* **6**, 219, doi:10.3389/fimmu.2015.00219 (2015).

8 Ramel, D. *et al. Shigella flexneri* infection generates the lipid PI5P to alter endocytosis and prevent termination of EGFR signaling. *Sci Signal* **4**, ra61, doi:10.1126/scisignal.2001619 (2011).

9 Ferrari, M. L. *et al. Shigella* promotes major alteration of gut epithelial physiology and tissue invasion by shutting off host intracellular transport. *Proc Natl Acad Sci U S A* **116**, 13582-13591 (2019).

10 Kobayashi, T. *et al.* The *Shigella* OspC3 effector inhibits caspase-4, antagonizes inflammatory cell death, and promotes epithelial infection. *Cell Host Microbe* **13**, 570-583 (2013).

11 Carneiro, L. A. *et al. Shigella* induces mitochondrial dysfunction and cell death in nonmyleoid cells. *Cell Host Microbe* **5**, 123-136 (2009).

12 Bergounioux, J. *et al.* Calpain activation by the *Shigella flexneri* effector VirA regulates key steps in the formation and life of the bacterium's epithelial niche. *Cell Host Microbe* **11**, 240-252 (2012).

13 Niebuhr, K. *et al.* Conversion of PtdIns(4,5)P-2 into PtdIns(5)P by the *S. flexneri* effector IpgD reorganizes host cell morphology. *Embo J* **21**, 5069-5078 (2002).

14 Pendaries, C. *et al.* PtdIns5P activates the host cell PI3-kinase/Akt pathway during *Shigella flexneri* infection. *Embo J* **25**, 1024-1034 (2006).

15 Willingham, S. B. *et al.* Microbial pathogen-induced necrotic cell death mediated by the inflammasome components CIAS1/Cryopyrin/NLRP3 and ASC. *Cell Host & Microbe* **2**, 147-159 (2007).

16 Suzuki, T. et al. Differential regulation of caspase-1 activation, pyroptosis, and autophagy via Ipaf and ASC in *Shigella*-infected macrophages. PloS Pathog **3**, 1082-1091 (2007).

17 Suzuki, S. et al. *Shigella* type III secretion protein MxiI is recognized by Naip2 to induce Nlrc4 inflammasome activation independently of Pkcδ. PLoS Pathog **10**, e1003926 (2014).

18 Runyen-Janecky, L. J. & Payne, S. M. Identification of chromosomal *Shigella flexneri* genes induced by the eukaryotic intracellular environment. Infect Immun **70**, 4379-4388 (2002).

19 Doench, J. G. *et al.* Optimized sgRNA design to maximize activity and minimize off-target effects of CRISPR-Cas9. *Nat Biotechnol* **34**, 184-191 (2016).

20 Sanson, K. R. *et al.* Optimized libraries for CRISPR-Cas9 genetic screens with multiple modalities. *Nat Commun* **9**, 5416, doi:10.1038/s41467-018-07901-8 (2018).

21 Lai, Y. *et al.* Illuminating host-mycobacterial interactions with functional genomic screening to inhibit mycobacterial pathogenesis. *bioRxiv*, 2020.2003.2030.016139, doi:10.1101/2020.03.30.016139 (2020).

22 Gaudet, R. G. *et al.* Innate recognition of intracellular bacterial growth is driven by the TIFA-dependent cytosolic surveillance pathway. *Cell Rep* **19**, 1418-1430 (2017).

23 Garcia-Weber, D. *et al.* ADP-heptose is a newly identified pathogen-associated molecular pattern of *Shigella flexneri*. *Embo Reports* **19**, doi:ARTN e46943 10.15252/embr.201846943 (2018).

24 Milivojevic, M. *et al.* ALPK1 controls TIFA/TRAF6-dependent innate immunity against heptose-1,7-bisphosphate of gram-negative bacteria. *PLoS Pathog* **13**, e1006224, doi:10.1371/journal.ppat.1006224 (2017).

25 Zhou, P. *et al.* Alpha-kinase 1 is a cytosolic innate immune receptor for bacterial ADP-heptose. *Nature* **561**, 122-126 (2018).

26 Kentner, D. *et al. Shigella* reroutes host cell central metabolism to obtain high-flux nutrient supply for vigorous intracellular growth. *Proc Natl Acad Sci USA* **111**, 9929-9934 (2014).

27 Senerovic, L. *et al.* Spontaneous formation of IpaB ion channels in host cell membranes reveals how *Shigella* induces pyroptosis in macrophages. *Cell Death Dis* **3**, doi:ARTN e384 10.1038/cddis.2012.124 (2012).

28 Suzuki, S. *et al. Shigella* IpaH7.8 E3 ubiquitin ligase targets glomulin and activates inflammasomes to demolish macrophages. *Proc Natl Acad Sci USA* **111**, E4254-E4263 (2014).

29 He, S., Liang, Y., Shao, F. & Wang, X. Toll-like receptors activate programmed necrosis in macrophages through a receptor-interacting kinase-3-mediated pathway. *Proc Natl Acad Sci U S A* **108**, 20054-20059 (2011).

30 Wee, Z. N. *et al.* IRAK1 is a therapeutic target that drives breast cancer metastasis and resistance to paclitaxel. *Nat commun* **6**, 1-16 (2015).

31 Oliveira-Nascimento, L., Massari, P. & Wetzler, L. M. The role of TLR2 in infection and immunity. *Front Immunol* **3**, 79, doi:10.3389/fimmu.2012.00079 (2012).

32 Wiersinga, W. J. *et al.* Toll-like receptor 2 impairs host defense in gram-negative sepsis caused by *Burkholderia pseudomallei* (Melioidosis). *PLoS Med* **4**, e248, doi:10.1371/journal.pmed.0040248 (2007).

33 Spiller, S. *et al.* TLR4-induced IFN-gamma production increases TLR2 sensitivity and drives Gram-negative sepsis in mice. *J Exp Med* **205**, 1747-1754 (2008).

34 Miao, E. A. *et al.* Caspase-1-induced pyroptosis is an innate immune effector mechanism against intracellular bacteria. *Nature Immunology* **11**, 1136-U1194 (2010).

35 Liu, X. *et al.* Inflammasome-activated gasdermin D causes pyroptosis by forming membrane pores. *Nature* **535**, 153-158 (2016).

36 Gu, B. *et al.* Comparison of the prevalence and changing resistance to nalidixic acid and ciprofloxacin of *Shigella* between Europe-America and Asia-Africa from 1998 to 2009. *Int J Antimicrob Agents* **40**, 9-17 (2012).

37 World Health Organization & Unicef. *Ending preventable child deaths from pneumonia and diarrhoea by 2025: The integrated Global Action Plan for Pneumonia and Diarrhoea (GAPPD)*. World Health Organization: Geneva (2013).

38 Chen, S. *et al.* Genome-wide CRISPR screen in a mouse model of tumor growth and metastasis. *Cell* **160**, 1246-1260 (2015).

39 Raudvere, U. *et al.* g:Profiler: a web server for functional enrichment analysis and conversions of gene lists (2019 update). *Nucleic Acids Res* **47**, W191-W198 (2019).

40 Merico, D., Isserlin, R., Stueker, O., Emili, A. & Bader, G. D. Enrichment map: a network-based method for gene-set enrichment visualization and interpretation. *PLoS One* **5**, e13984, doi:10.1371/journal.pone.0013984 (2010).

41 Zhong, W. *et al.* Allosteric pyruvate kinase-based "logic gate" synergistically senses energy and sugar levels in *Mycobacterium tuberculosis*. *Nat Commun* **8**, 1986, doi:10.1038/s41467-017-02086-y (2017).

Methods

Reagents

IRAK1/4-Inh (I5409), oxythiamine, and ginsenoside Compound K were purchased from Sigma and used at the following concentrations: IRAK1/4-Inh, 0.1-10 μM; Oxythiamine, 0.01-1 mM; Compound K, 1-25 μM. Antibiotics in the media were at the following

362 concentrations: 100 μg ml^{-1} ampicillin, 100 μg ml^{-1} gentamicin, 100 U ml^{-1} Penicillin-
363 Streptomycin (Pen/Strep; Gibco).

364 **Mammalian cell culture**

365 The human monocyte cell line THP-1 was a gift from Jianzhu Chen (Singapore-MIT
366 Alliance for Research and Technology). HEK293FT cells were gifts from Asha Shekaran
367 (Engine Biosciences). THP-1 cells were cultured in RPMI1640 (HyClone) with 10% FBS
368 (Gibco) and Pen/Strep at 37°C with 5% CO_2. 50 ng ml^{-1} phorbol 12-myristate 13-acetate
369 (PMA; Sigma) was used to differentiate THP-1 cells in tissue culture treated 96-well plates
370 (Corning). HEK293FT cells were cultured in Dulbecco's modified Eagle's medium
371 (DMEM) (HyClone) supplemented with 10% FBS and Pen/Strep at 37°C with 5% CO_2.

372 **Bacterial strains and growth conditions**

373 *Shigella flexneri* M90T *ΔvirG* pCK100 (P*uhpT*::dsRed), a gift from Cecile Arrieumerlou
374 (Institut Cochin), was grown in Lysogeny broth (LB) medium overnight at 37°C with
375 shaking. The next day, bacteria were diluted 1:100 into 10 mL LB medium and grown to
376 exponential phase for infection. When necessary, 100 μg ml^{-1} ampicillin was added to the
377 growth medium.

378 ***In vitro* bacterial infection**

379 *S. flexneri* M90T *ΔvirG* pCK100 were prepared in exponential growth phase for host cell
380 infection. THP-1 cells were infected at an MOI of 10 in complete RPMI1640 medium at
381 indicated times. To test the combination of IRAK1 and PDHB small molecule inhibitors,
382 THP-1 cells were infected at an MOI of 1:10. After *Shigella* infection, THP-1 cells were
383 treated with 100 μg ml^{-1} gentamicin for 2 hours to kill extracellular bacteria. Subsequently,

384 host cells were washed and maintained for the rest of the experiments. Viable THP-1 cells
385 were counted in a hemocytometer by using trypan blue (Gibcon). Cell death of PMA-
386 stimulated THP-1 cells were measured by LDH assay (Takara).

387 **Enumeration of intracellular bacteria in infected cells**

388 At selected time points, 1 ml of *Shigella*-infected THP-1 cells were centrifuged and washed
389 twice with 1×PBS and then lysed with 50 µl of 1×PBS with 1% Triton 100. PMA-
390 stimulated THP-1 cell infected with *S. flexneri* were lysed with 50 µl of 1×PBS with 1%
391 Triton 100. 10-fold serial dilutions were performed followed by plating on LB agar plates
392 and incubated at 37°C for 24 hours. The number of viable intracellular bacteria was
393 calculated from the counted colony forming unit (CFU) on the agar plates.

394 **Pooled Genome-wide and secondary CRISPR Screens**

395 The Brunello human CRISPR knockout pooled library was obtained from Addgene
396 (#73178). The Dolcetto human CRISPRi pooled library was a gift from John Doench (the
397 Broad Institute, also available on Addgene #92385). Both secondary CRISPR knockout
398 and CRISPRi libraries, with 10 sgRNAs per gene, were designed to target the 251 genes
399 scored in primary genome-wide screens (133 of these genes were identified as being
400 involved in *S. flexneri* infection) and 121 genes from literature (47 of these genes were
401 found to be involved in *S. flexneri* infection)[21]. 1000 non-targeting sgRNAs were used as
402 controls[21].

403 **Lentiviral library packaging**

404 Well dissociated HEK293FT cells were seeded at a density of 1.4×10^7 cells per flask in a
405 total volume of 35 ml of DMEM medium 24 h before transfection. Cells were optimal for

transfection at 80-90% confluency using 7 ml of Opti-MEM, 231 µl of PLUS reagent, 210 µl of Lipofectamine 2000, and a DNA mixture of 18.2 µg of psPAX2 (Addgene #12260), 11.9 µg of pMD2.G (Addgene #12259), and 23.8 µg of library plasmid. Flasks were incubated at 37°C with 5% CO_2 for 4 hours. The media was replaced with 35 ml DMEM medium with 10% FBS and 1% BSA. Lentivirus was harvested 2 days after the start of transfection and filtered through a 0.45 µm polyethersulfone membrane.

Lentivirus transduction

To ensure that only one gene was targeted in each cell, Cas9- and dCas9-Krab-expressing THP-1 cells were transduced with the pooled lentiviral CRISPR knockout and CRISPRi libraries in three biological replicates at an MOI of 0.3, respectively. To ensure that each perturbation would be fully represented and reduce spurious effects due to random genome integration in the transduced cell population, screening libraries were prepared with coverage of >500 cells per sgRNA. Lentiviral spinfection was performed by centrifuging 12-well plates at 1,000 *g* for 2 hours at 33°C with THP-1 cells grown in RPMI1640 medium with 10% FBS and 8 µg ml^{-1} of polybrene. 24 hours after lentiviral transduction, cell culture medium was replaced by RPMI1640 with 10% FBS and 2 µg ml^{-1} of puromycin for selection. Following antibiotic selection, a library coverage of >3000× was maintained for subsequent screens.

CRISPR screens

After puromycin selection, each CRISPR library replicate was split, one for *Shigella* infection and one used as control to verify library representation. 100 µg ml^{-1} of gentamicin was added to the cell culture to kill extracellular pathogen post-infection. Surviving host

cells were harvested and pelleted by centrifugation with coverage of >500 cells per sgRNA. The pooled screens were performed as three independent replicates.

Genomic DNA extraction, barcode amplification, next generation sequencing (NGS), and analysis

Genomic DNA (gDNA) from live THP-1 cells was isolated using a homemade modified salt precipitation method as described previously[38]. The sgRNA cassette was amplified by PCR and prepared for Illumina sequencing (HiSeq2000) as described previously[20]. The sequencing reads were deconvoluted to generate a matrix of read counts, which were then normalized under each condition by the following formula: log2 (Reads per sgRNA/total reads per condition*10^6+1). The log2 fold change of each sgRNA was determined by comparing infected sample and uninfected samples for each biological replicate. A CRISPR screen analysis tool developed by the Genetic Perturbation Platform (GPP) at the Broad institute was used to evaluate the rank and statistical significance of genes (https://portals.broadinstitute.org/gpp/public/analysis-tools/crispr-gene-scoring). A hypergeometric distribution was used to calculate the overlap probability of screen hits between CRISPR knockout and CRISPRi screens. Tests were carried out in R package using the function phyper (q, m, n, k, lower. tail=FALSE), where q is the number of overlap genetic hits, m is the number of genetic hits identified by the CRISPR knockout screen, n is the total number of genes in the library, and k is the number of genetic hits identified by the CRISPRi screen. The g:Profiler tool[39] was used to perform gene-set enrichment analysis based on genetic hits identified by CRISPR screens. The KEGG, Reactome, and the Gene Ontology (Biological Process) were used as the pathway databases to identify gene sets. Enrichment Map was used for interpretation of the biological processes[40].

Validation of individual sgRNAs

For each sgRNA cloning, spacer-encoding sense and antisense oligonucleotides with BsmBI-compatible overhangs were synthesized, annealed, cloned into the lentiGuide-Puro vector (Addgene #52963), and verified by sequencing (Supplementary Table 5). Lentivirus was generated in HEK293FT cells using PLUS reagents and Lipofectamine 2000, following manufacturer's instructions. Lentiviral transduction was performed in dCas9-Krab-expressing THP-1 cells to generate individual gene knockdown THP-1 cells. After 11 days of puromycin selection, each individual gene knockdown THP-1 cell was infected with *S. flexneri* to validate its phenotype, such as host cell survival and intracellular pathogen growth, as a top positive genetic hit identified by the CRISPR screens.

Cytokine quantification

Supernatants of cell cultures were collected at indicated times post-bacterial infection. Cytokine and chemokine levels in *S. flexneri*-infected supernatants were determined using Bio-plex pro human cytokine 17-plex and IFN-a2 kit (Bio-Rad) according to the manufacturer's instructions. The results were measured by a Bio-Plex 200 system (Bio-Rad).

Metabolite profiling

Metabolite extraction and targeted metabolomics analyses followed the published reports with modifications[41]. Briefly, cell cultures were harvested at given time points and rapidly quenched, and metabolites were extracted using acetonitrile:methanol:water (2:2:1). After centrifugation, the supernatant was collected and evaporated to dryness in a vacuum

472 evaporator, and the dry extracts were redissolved in 100 µL of 98:2 water/methanol for
473 liquid chromatography-mass spectrometry (LC-MS) analysis.

474 The targeted LC-MS/MS analysis was performed with Agilent 1290 ultrahigh
475 pressure liquid chromatography system coupled to a 6490 Triple Quadrupole mass
476 spectrometer equipped with a dual-spray electrospray ionization source with Jet StreamTM
477 (Agilent Technologies, Santa Clara, CA). Chromatographic separation of metabolites in
478 central carbon metabolism was achieved by using Phenomenex (Torrance, CA) RezexTM
479 ROA-Organic Acid H+ (8%) column (2.1×100 mm, 3 µm) and the compounds were eluted
480 at 40°C with an isocratic flow rate of 0.3 mL min^{-1} of 0.1% formic acid in water.
481 Compounds were quantified in multiple reaction monitoring (MRM) mode. Electrospray
482 ionization was performed in both positive and negative ion modes with the following
483 source parameters: drying gas temperature 300°C with a flow of 10 L min^{-1}, nebulizer gas
484 pressure 40 psi, sheath gas temperature 350°C with a flow of 11 L min^{-1}, nozzle voltage
485 500 V, and capillary voltage 4,000 V and 3,000 V for positive and negative mode,
486 respectively. Data acquisition and processing were performed using MassHunter software
487 (Agilent Technologies, US), and cell counts were normalized to correct variations in
488 sample preparation.

489 **Imaging**

490 To visualize intracellular RFP-reporter *S. flexneri* M90T Δ*virG* (*uhpT*::dsRed), infected
491 THP-1 cells were directly observed under a confocal fluorescence microscope (Zeiss LSM
492 700).

493

Acknowledgements

We thank Karen Pepper for editing the manuscript. We thank Prof. Peter Dedon for reviewing the manuscript. This work was supported by the United States Defense Threat Reduction Agency (HDTRA1-15-1-0050 to T.K.L.), and the National Research Foundation of Singapore through the Singapore-MIT Alliance for Research and Technology AMR IRG (Y.L., L.C., T.K.L.)

Author contributions Y.L., L.C., J.G.D., and T.K.L. conceived and designed the research; Y.L. and J.G.D. performed and analyzed genome-wide CRISPR screen experiments; Y.L. and J.G.D. designed, performed and analyzed secondary CRISPR screen experiments; Y.L. conducted validation experiments of genetic hits and small molecule inhibitors; Y.L. and L.C. designed and performed metabolite profile experiments; Y.L. and T.K.L. coordinated the overall research; T.K.L. supervised the overall research; Y.L., L.C., J.G.D., and T.K.L. analyzed the data and wrote the manuscript. All authors discussed the results and reviewed the paper.

Competing interests

T.K.L. is a co-founder of Senti Biosciences, Synlogic, Engine Biosciences, Tango Therapeutics, Corvium, BiomX, and Eligo Biosciences. T.K.L. also holds financial interests in nest.bio, Ampliphi, IndieBio, MedicusTek, Quark Biosciences, and Personal Genomics.

Y.L. and T.K.L. are co-inventors on a US provisional patent application (no. 62/909727), which is based on discoveries described in this paper.

Supplementary Information is available in the online version of the paper.

Correspondence and requests for materials should be addressed to T.K.L.

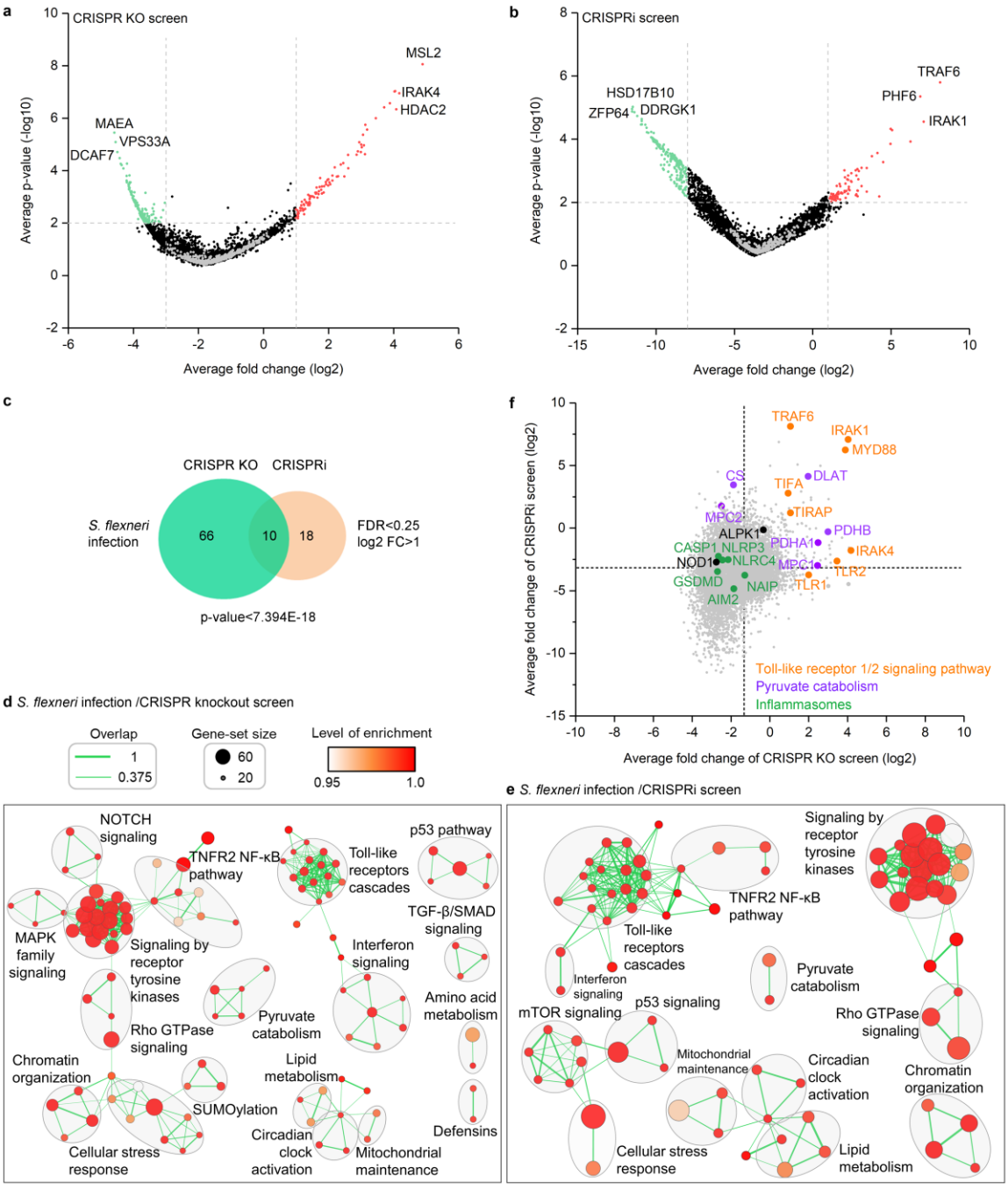

Fig. 1 Genome-wide pooled CRISPR knockout and CRISPRi screens to dissect biological pathways in *S. flexneri* infection. a and **b**, Volcano plots from CRISPR knockout (**a**) and CRISPRi (**b**) screens. For each sgRNA-targeted gene, the x axis shows its enrichment (positive hits) or depletion (negative hits) post-infection, and the y axis

shows statistical significance measured by p-value. Top 3 positive and negative screen hits are labeled as red and green dots, respectively. Gray dots represent non-targeting controls. For each screen, experiments were carried out in triplicates. **c**, Enriched genes in Venn diagram were filtered with a cut-off of FDR <0.25 and log2 fold change >1 in *S. flexneri* infection. The degree of significance of the overlap is given. **d** and **e**, Candidate genes identified by CRISPR knockout and CRISPRi screens were functionally categorized to understand the biological functions involved in *S. flexneri* infection. Edge width represents mutual overlap of genes. Node size represents the number of genes in the gene set. Color gradient of nodes represents the enrichment scores of gene-sets. **f**, Gene-centric visualization of average log2 fold change of CRISPR knockout and CRISPRi screens in *S. flexneri*-infected versus non-infected host cells. Selected components of TLR1/2, pyruvate catabolism signaling pathway, and inflammasome formation are highlighted in orange, purple, and green.

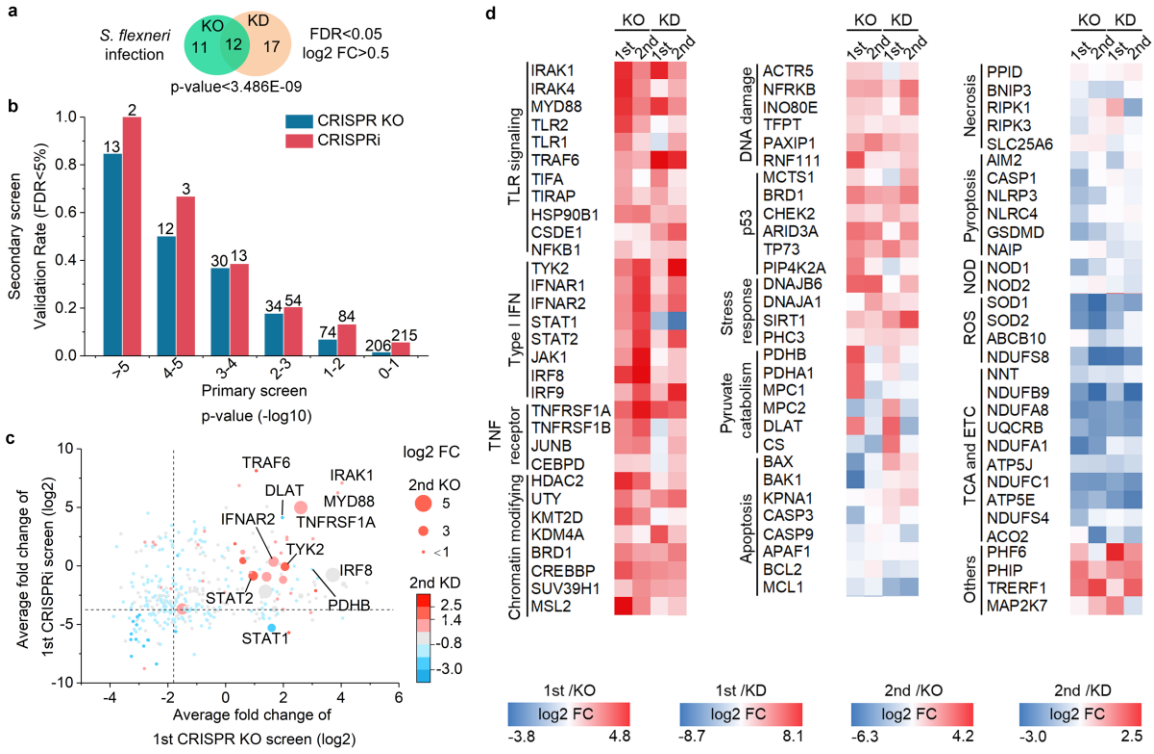

560

561 **Fig. 2 Secondary CRISPR knockout and CRISPRi screens identify host genetic hits**
562 **in *S. flexneri* infection. a**, Enriched genes were filtered with a cut-off of FDR <0.05 and
563 log2 fold change >0.5 in *S. flexneri* infection. The degree of significance of the overlap is
564 given. **b**, Validation rate of genetic hits in the secondary screen grouped by their p-value
565 in the genome-wide screens in *S. flexneri* infection. Number of genes per category is
566 indicated. **c**, Genetic hits from both primary and secondary screens were ranked by their
567 differential gRNA abundance between *S. flexneri*-infected versus uninfected populations
568 (log2 fold change). **d**, Heatmap of screen hits clustered in different biological pathways in
569 *S. flexneri* infection.

570

571

572

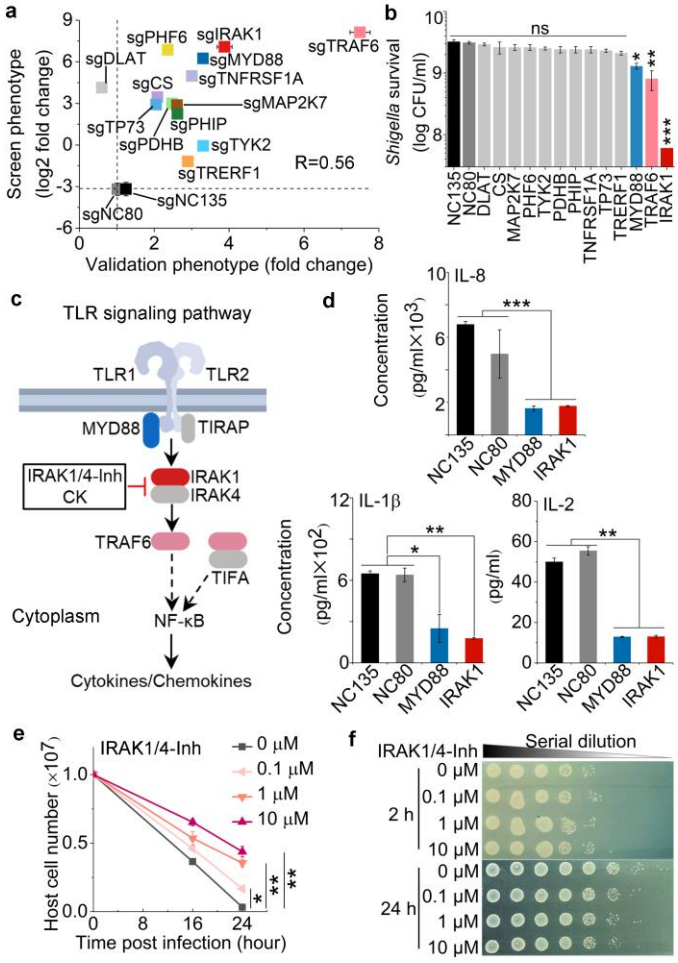

Fig. 3 Validation of top positive genetic hits and IRAK1 inhibitor in *S. flexneri* infection of human THP-1 cells. **a**, Correlation between pooled screen and validation data. For each hit, the log2 fold change obtained from the genome-wide screening data (Screen phenotype) was plotted against the fold-change of cell viability of genetic hits compared to the non-targeting control cells (Validation phenotype). sgNC80 and sgNC135 are non-targeting controls. R is the Pearson correlation coefficient. **b**, Intracellular *S. flexneri* level after infection of individual knockdown THP-1 cells. **c**, Schematic of positive genetic hits in TLR1/2 signaling pathway and corresponding inhibitors. **d**, Cytokine and chemokine production in MYD88 and IRAK1 knockdown THP-1 cells post-infection. **e** and **f**, The viability of THP-1 cells (**e**) and intracellular *Shigella* growth (**f**) post-infection in the

presence or absence of IRAK1 inhibitor at different concentrations. Data represent the mean ± SD (n = 3) (two-tailed unpaired Student's *t*-test, * P<0.05 ** P<0.01 *** P<0.001; ns represents not significant).

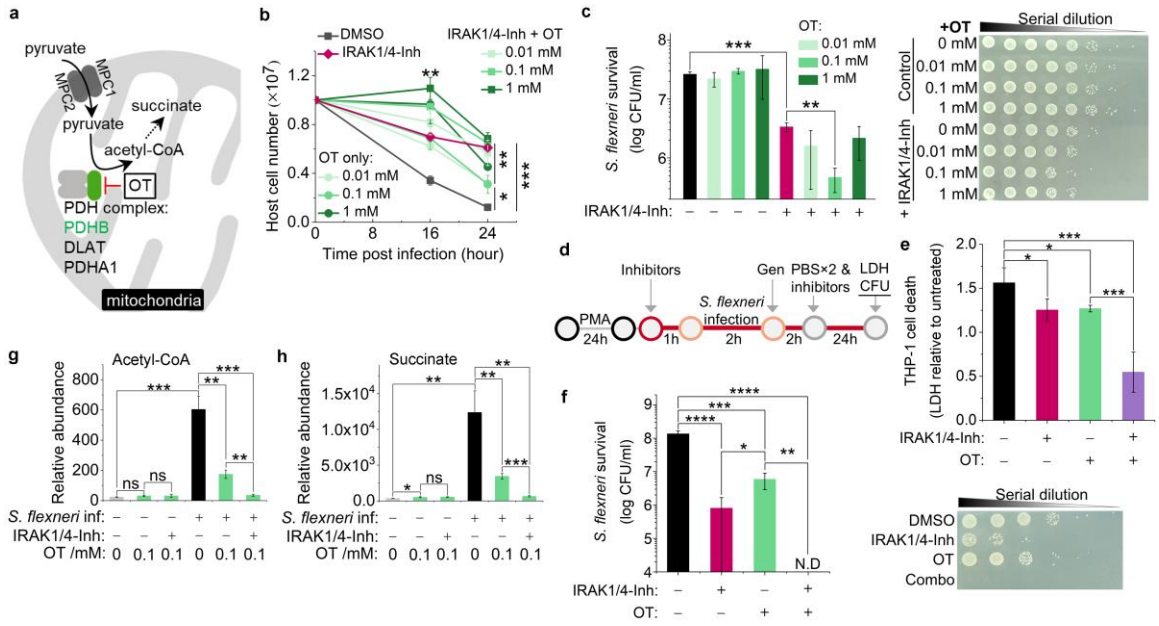

Fig. 4 Validation of positive genetic hits in pyruvate catabolism signaling pathway and corresponding inhibitor in *S. flexneri* infection of human THP-1 cells. **a**, Schematic of positive genetic hits in pyruvate catabolism signaling pathway and corresponding inhibitor. **b** and **c**, The growth of THP-1 cells (**b**) and intracellular *S. flexneri* level (**c**) post-infection in the presence or absence of different concentrations of PDHB inhibitor (OT) and combined with IRAK1/4-Inh. **d**, Schematic of inhibitor validation in PMA-stimulated THP-1 cell infected with *S. flexneri*. **e**, Effects of IRAK1 and PDHB inhibitors on the survival of differentiated THP-1 post-infection, with death measured by lactate dehydrogenase (LDH) release relative to the untreated condition. **f**, Effects of IRAK1 and PDHB inhibitors on the growth of intracellular *S. flexneri* in differentiated THP-1 cells. IRAK1/4-Inh is used at 10 μM. OT is used at 0.1 μM. **g** and **h**, Production of acetyl-CoA (**g**) and succinate (**h**) with or without *S. flexneri* infection and in the presence or absence of OT and combined with IRAK1 inhibitor. Data represent the mean ± SD (**b**, **c**, **g** and **h**, n = 3; **e** and **f**, n = 4) (two-tailed unpaired Student's *t*-test, * P<0.05 ** P<0.01 *** P<0.001 **** P<0.0001; ns represents not significant; N.D represents not detectable).

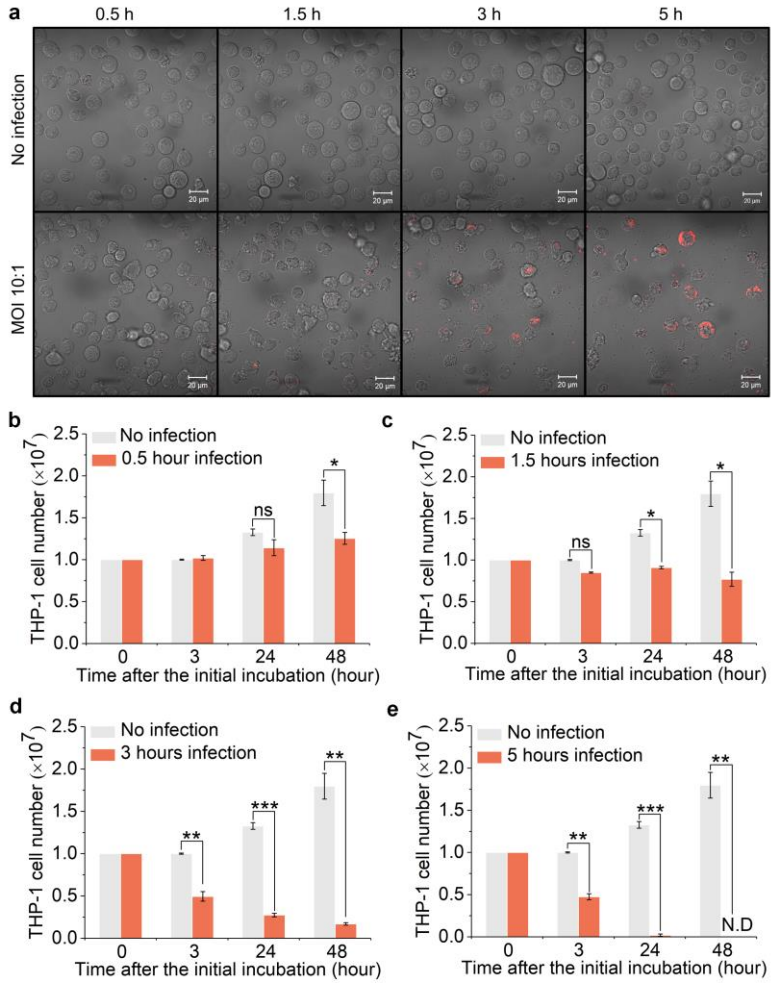

Extended Data Fig. 1 Optimization of conditions for *Shigella* infection of THP-1 cells. **a**, *S. flexneri* infection at an MOI (number of bacterial cells per host cell) of 10, from 0.5 hour to 5 hours incubation with THP-1 cells (Scale bar, 20 μm). **b-e**, The number of *Shigella*-infected THP-1 cells after 0.5 to 5 hours infection. More than 90% of host cells were killed after 3 hours of infection (**d**). N.D represents not detectable. Data represent mean ± SD (n = 3) (two-tailed unpaired Student's *t*-test, * P<0.05 ** P<0.01 *** P<0.001; ns represents not significant).

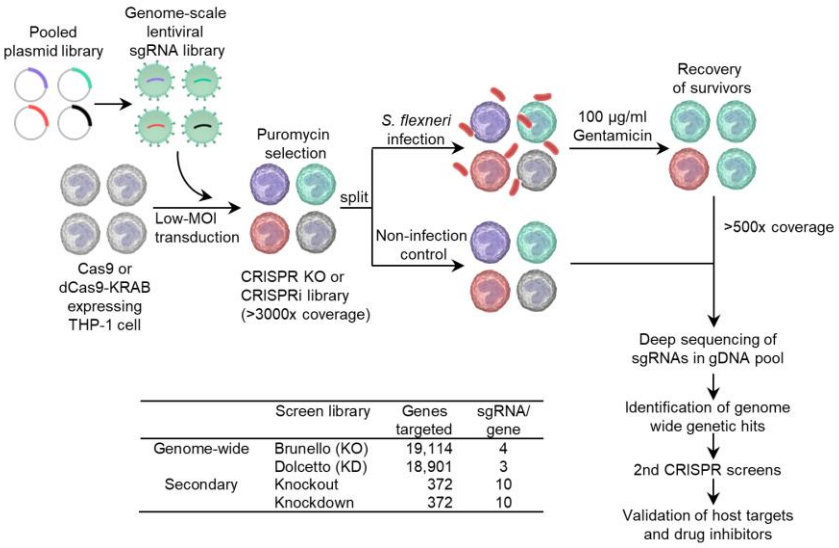

	Screen library	Genes targeted	sgRNA/ gene
Genome-wide	Brunello (KO)	19,114	4
	Dolcetto (KD)	18,901	3
Secondary	Knockout	372	10
	Knockdown	372	10

Extended Data Fig. 2 Strategy for preparing CRISPR screen libraries and performing positive screens. Monoclonal Cas9 and dCas9-Krab-expressing THP-1 cell lines were constructed and transduced with lentiviral sgRNA libraries[21]. High coverage CRISPR knockout and CRISPRi libraries were split for subsequent *S. flexneri* infection. Surviving THP-1 cells with sgRNA barcodes were harvested and processed for next generation sequencing. Genome-wide genetic hits were identified by comparing sgRNA abundance between infected samples and non-infected controls. Based on those host targets, secondary CRISPR knockout and CRISPRi screen libraries were designed and prepared[21]. Similarly, secondary positive screens were performed to validate those host targets. Finally, drug inhibitors which selectively inhibit genetic hits were tested.

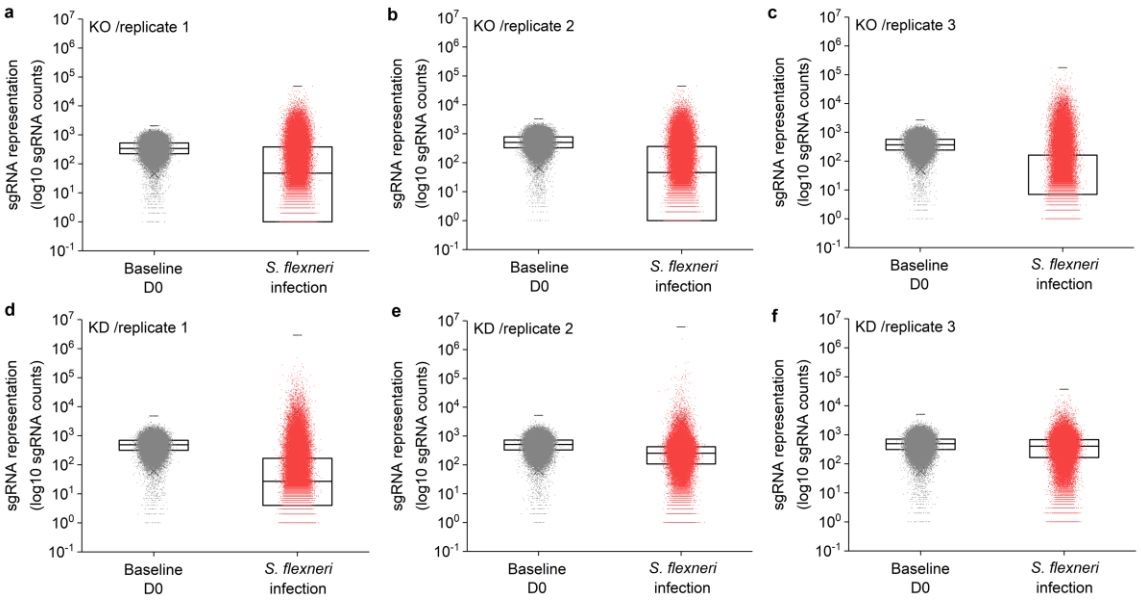

644

645 **Extended Data Fig. 3 sgRNA distribution of CRISPR knockout and CRISPRi**
646 **screening. a-c,** Distribution of individual sgRNA in control and *S. flexneri*-infected
647 samples after CRISPR knockout screens. **d-f**, Distribution of individual sgRNA in control
648 and *S. flexneri*-infected samples after CRISPRi screens. Each point represents individual
649 sgRNAs. Boxes, 25th to 75th percentile; Whiskers, 1st to 99th percentile.

650

651

652

653

654

655

656

657

a CRISPR KO screen

Biological pathways	p-value (-log10)
Regulation of IFNA signaling	7.2
Toll-Like receptors cascades	7.2
Class I MHC mediated antigen processing & presentation	6.2
Pyruvate metabolism	6.0
Chromatin organization	5.9
RHO GTPases activate WASPs and WAVEs	5.6
NOTCH1 intracellular domain regulates transcription	5.2
Transcriptional regulation by TP53	5.2
Regulation of pyruvate dehydrogenase (PDH) complex	5.0
Signaling by SCF-KIT	4.8
PI3K/AKT activation	3.8
Signaling by FGFR	3.8
Regulation of actin dynamics for phagocytic cup formation	3.8
Cellular responses to stress	3.8
Circadian clock	3.4
Signaling by TGF-beta receptor complex	3.4
Defensins	2.3
Metabolism of amino acids and derivatives	1.6

b CRISPRi screen

Biological pathways	p-value (-log10)
Chromatin organization	5.9
Toll Like Receptor 2 (TLR2) Cascade	5.4
PI3K/AKT activation	5.4
RHO GTPases activate WASPs and WAVEs	5.1
Signaling by SCF-KIT	4.6
Signaling by FGFR	4.5
Cellular responses to stress	4.5
Transcriptional regulation by TP53	3.7
Regulation of actin dynamics for phagocytic cup formation	3.6
mTORC1-mediated signaling	3.6
Fcgamma receptor (FCGR) dependent phagocytosis	3.4
TNFs bind their physiological receptors	3.4
Pyruvate metabolism and TCA cycle	3.0
Cytosolic sensors of pathogen-associated DNA	2.7
Circadian clock	2.7
Mitochondrial biogenesis	2.5
TNFR2 non-canonical NF-kB pathway	2.4
Regulation of lipid metabolism PPARalpha	2.3

Extended Data Fig. 4 Enrichment of biological pathways identified by genome-wide CRISPR knockout and CRISPRi screens in *S. flexneri* infection of THP-1 cells. a and **b,** Gene enrichment analysis of positive genetic hits identified by CRISPR knockout screen (**a**) and CRISPRi screen (**b**) in *S. flexneri* infection (FDR<0.1 and log2 FC>1).

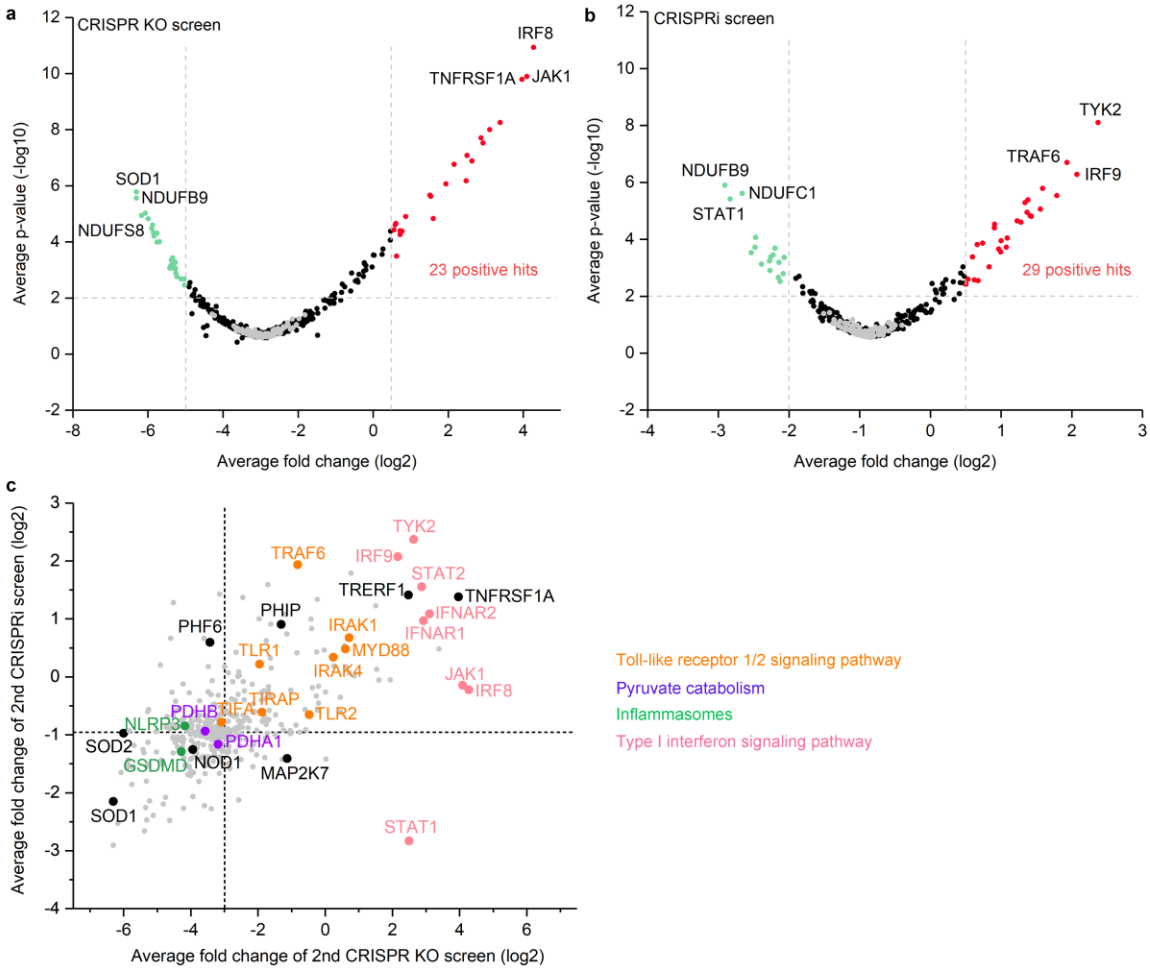

Extended Data Fig. 5 Genetic hits identified by secondary CRISPR screens in *Shigella* infection. **a** and **b,** Volcano plots from secondary CRISPR knockout (**a**) and CRISPRi (**b**) screens. For each sgRNA-targeted gene, the x axis shows its enrichment (positive hits) or depletion (negative hits) post-infection, and the y axis shows statistical significance measured by p-value. Top 3 positive and negative screen hits are labeled as red and green dots, respectively. Gray dots represent non-targeting controls. For each screen, experiments were carried out in triplicate. **c**, Gene-centric visualization of average fold change of secondary screens in *S. flexneri*-infected versus non-infected host cells. Selected components of TLR 1/2 signaling pathway, pyruvate catabolism, inflammasome formation,

680 and type I interferon signaling pathway are highlighted in orange, purple, green, and pink,
681 respectively.

682

683

684

685

686

687

688

689

690

691

692

693

694

695

696

697

698

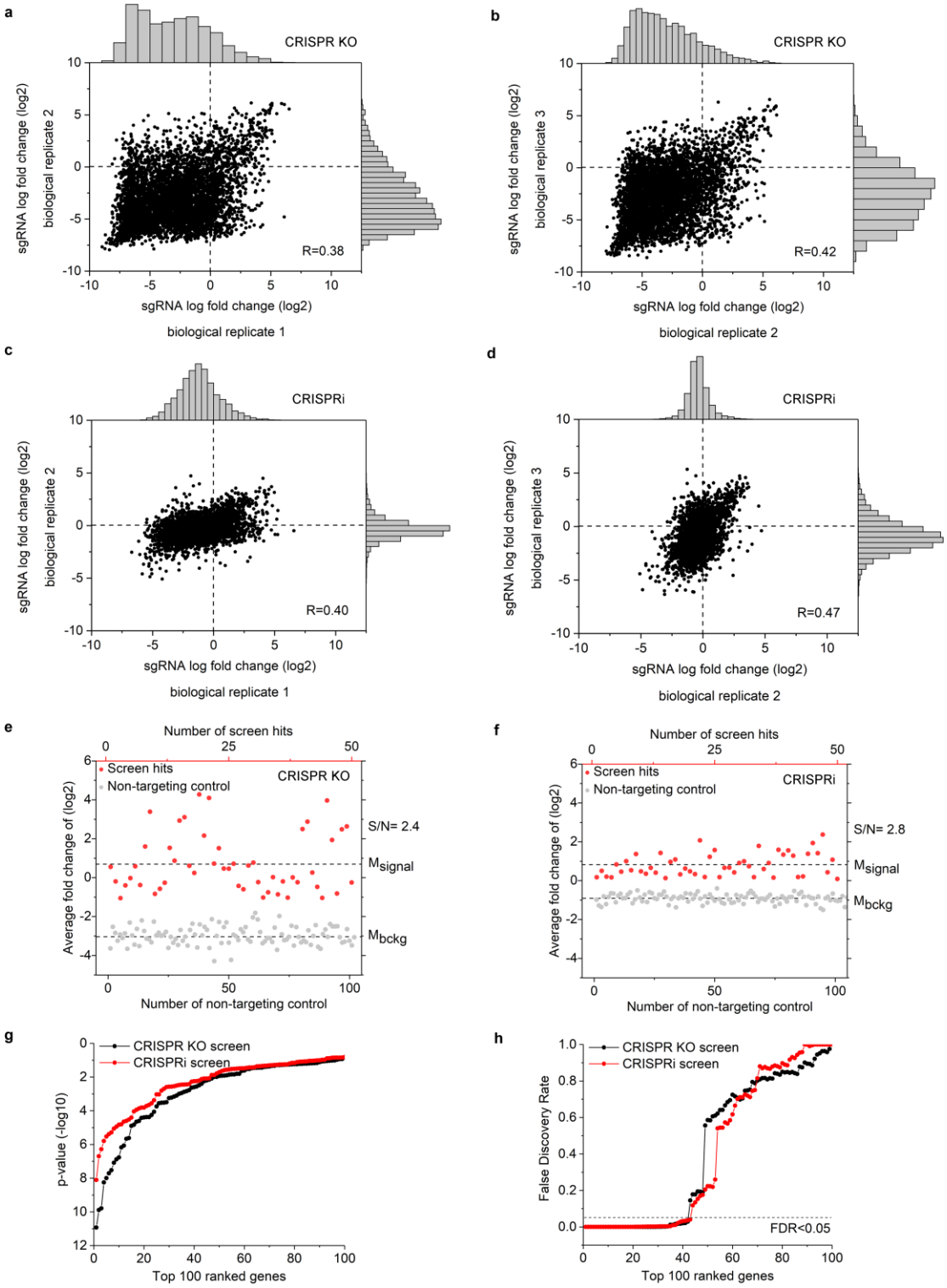

Extended Data Fig. 6 Comparison of secondary CRISPR knockout and CRISPRi screens in *S. flexneri* infection. **a-d**, sgRNA-level correlation of replicates in CRISPR

knockout screens (**a** and **b**) and CRISPRi screens (**c** and **d**). Pearson correlation of log2 fold change values between replicates is indicated. **e** and **f**, Top 50 positive genetic hits (red) and non-targeting controls (gray) identified by CRISPR knockout (**e**) and CRISPRi (**f**) in *S. flexneri* infection. Broken lines show the means of the hits (M_{signal}) and non-targeting controls (M_{bckg}). **g** and **h**, p-value (**g**) and FDR (**h**) of top 100 positive genetic hits identified by CRISPR knockout and CRISPRi screens in *S. flexneri* infection.

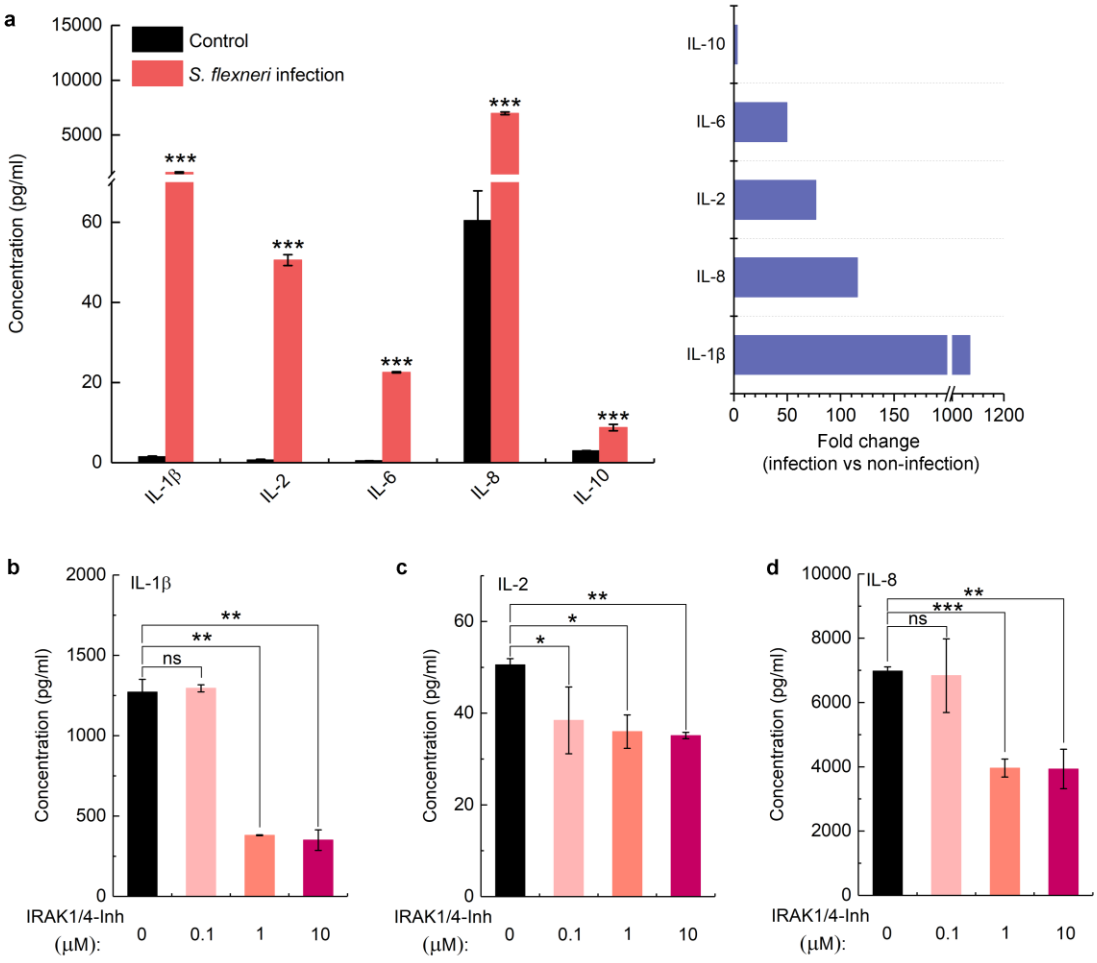

Extended Data Fig. 7 Cytokine and chemokine production in THP-1 cells in *S. flexneri* infection. **a**, Cytokine and chemokine production in THP-1 cells with or without *S. flexneri* infection. **b-d**, Production of IL-1β (**b**), IL-2 (**c**), and IL-8 (**d**) in THP-1 cells in the presence of IRAK1 inhibitor at different concentrations. Data represent the mean ± SD (n = 3) (two-tailed unpaired Student's *t*-test, * P<0.05 ** P<0.01 *** P<0.001; ns represents not significant).

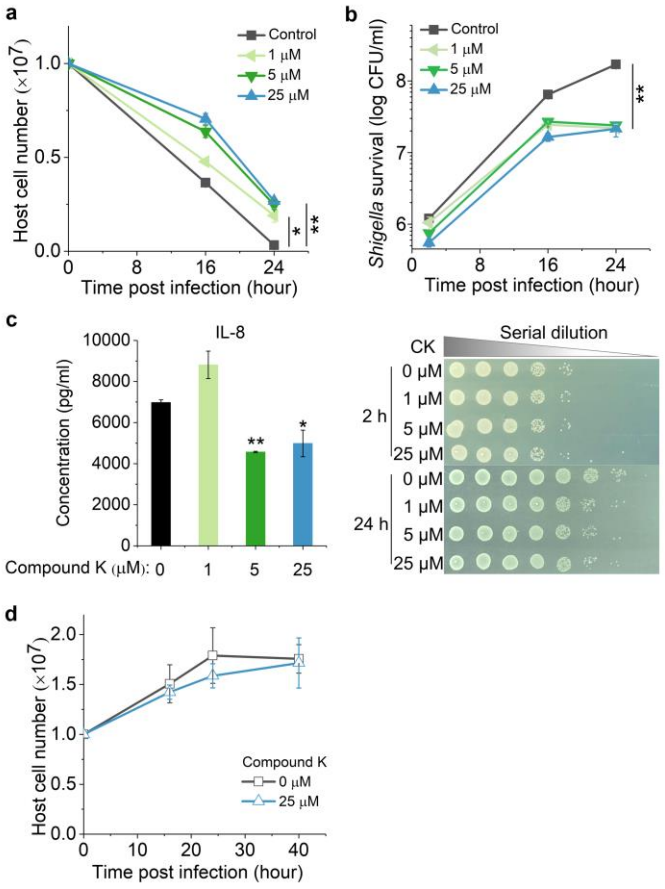

731

732 **Extended Data Fig. 8 Validation of IRAK1 inhibitor Compound K in *Shigella***
733 **infection**. **a**, Survival of THP-1 cells post-infection in the presence or absence of different
734 concentrations of Compound K (CK). **b**, Intracellular *S. flexneri* growth in the presence or
735 absence of different concentrations of CK. **c**, Production of infection-induced IL-8 in the
736 presence or absence of different concentrations of CK. **d**, The growth of THP-1 cells in the
737 presence or absence of CK without *S. flexneri* infection. Data represent the mean ± SD (n
738 =3) (two-tailed unpaired Student's *t*-test, * P<0.05 ** P<0.01; ns represents not significant).